Buckling analysis of functionally graded porous variable thickness plates resting on Pasternak foundation using ES-MITC3

Truong Thanh Nguyen[a] (iD) **, Truong Son Le[b]** (iD) **, Trung Thanh Tran[b]** (iD) **, Quoc-Hoa Pham[c*]** (iD)

[a]Air Force Officer's College, Nha Trang, Khanh Hoa, Vietnam. Email: truongthanhna74@gmail.com
[b]Faculty of Mechanical Engineering, Le Quy Don Technical University, Hanoi, Vietnam. Emails: letruongson01@gmail.com; tranthanh0212@gmail.com
[c]Faculty of Engineering and Technology, Nguyen Tat Thanh University, Ho Chi Minh City, Vietnam. Email: pqhoa@ntt.edu.vn

*Corresponding author.
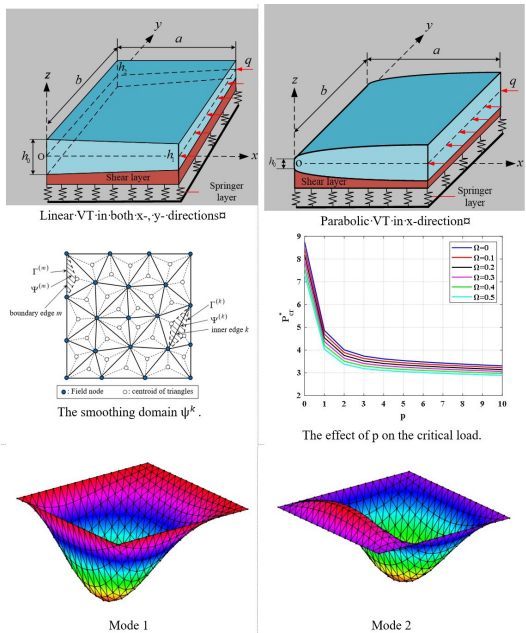
https://doi.org/10.1590/1679-78257886

Abstract

The main goal of this study is to further expand the ES-MITC3 for analyzing the buckling characteristics of functionally graded porous (FGP) variable thickness (VT) plates with sinusoidal porous distribution. The ES-MITC3 was developed to improve the accuracy of classical triangular elements (Q3) and overcome the locking phenomenon while still ensuring flexibility in discretizing the structural domain of the Q3. The first-order shear deformation theory (FSDT) in combination with ES-MITC3 is used due to its simplicity and effectiveness. The Pasternak foundation (PF) is a two-parameter model with springer stiffness (k_1) and shear stiffness (k_2) that describes the foundation reaction as a function of the deflection and its Laplacian. The accuracy and performance of the proposed formulation are verified through comparative examples. Moreover, a comprehensive analysis has been undertaken to scrutinize the effects of geometric parameters and material properties on the buckling of FGP VT plates.

Keywords

FGP, buckling analysis, variable thickness plate, ES-MITC3.

Graphical Abstract

Linear VT in both x-, y- directions¤

Parabolic VT in x-direction¤

The smoothing domain ψ^k.

The effect of p on the critical load.

Mode 1

Mode 2

Buckling analysis of functionally graded porous variable thickness plates resting on Pasternak foundation
using ES-MITC3

Truong Thanh Nguyen et al.

Nomenclature	
IGA	Isogeometric analysis
FEM	Finite element method
TSDT	Third-order shear deformation theory
HSDT	Higher-order shear deformation theory
FSDT	First-order shear deformation theory
FGM	Functionally graded material
FGP	Functionally graded porous
ES	Exact solution
BCs	Boundary conditions
MCST	Modified couples stress theory
TBT	Timoshenko beam theory
EF	Elastic Foundation
PF	Pasternak foundation
DOF	Degrees of freedom
Q3	The triangular element
ES-MITC3	The mixed interpolation of the tensorial components technique for the three-node triangular element (MITC3) combined with the edge-based smoothed finite element method (ES-FEM)

1 INTRODUCTION

The functionally graded porous (FGP) is a special form of the functionally graded materials (FGMs) (Ramu and Mohanty 2014; Saha and Maiti 2012; Wu et al. 2007; Javaheri and Eslami 2002; Zenkour 2005; Shariat and Eslami 2007; Thai and Choi 2012; Reddy et al. 2013; Thinh et al. 2016; Do and Tran 2023) with the appearance of pores inside, these pores can be distributed randomly or according to the law according to human intention. Despite the presence of many internal pores, FGP also exhibits impressive mechanical characteristics, including lightweight, exceptional energy absorption capabilities, and remarkable heat resistance properties. Several notable examinations have been conducted to analyze the mechanical behaviour of FGP structures, some of which include: Kim et al. (2019) used an exact solution (ES) to study the mechanical behaviour of FGP microplates based on modified couples stress theory (MCST). Chen et al. (2015) used Timoshenko beam theory (TBT) to study the buckling of FGP beams. Rezaei and Saidi (2016) analyzed the vibration of porous-cellular plates using Carrera unified formulation. Li et al. (2018) studied the nonlinear response of FGP plates based on both the Galerkin and the fourth-order Runge–Kutta methods. Wu et al. (2018) examined the dynamic behaviour of FGP plates using finite element method (FEM). Thang et al. (2018) used an ES to analyze the buckling of FGP plates, etc. Furthermore, readers can find the results of mechanical behavior analysis of FGP structures in available documents (Pham et al. 2022; Vu et al. 2023; Tran and Le 2023; Pham et al. 2023; Nguyen et al. 2023; Do et al. 2023; Nguyen et al. 2022; Tran et al. 2021).

Variable thickness (VT) structures are extensively employed in a wide range of high-performance surfaces, ranging from aerospace to civil engineering and many other engineering fields. The utilization of such structures plays a pivotal role in optimizing structural weight, thereby enhancing the material's load-bearing capacity to its maximum potential. Research on this structure can include some typical works such as Eisenberger and Alexandrov (2003) used the Kantorovich method to investigate the buckling of VT isotropic plates. Jalali et al. (2010) applied the pseudo-spectral method to analyze the buckling of the FGM VT circular sandwich plates. Benlahcen et al. (2018) based on ES to analyze the buckling of FGM VT plates. Bouguenina et al. (2015) examined the thermal buckling of FGM VT plates using an ES. Moreover, Zenkour (2018) studied the mechanical bending of VT plates employing Navier's solution. Banh-Thien et al. (2017) used isogeometric analysis (IGA) to examine the buckling of VT nanoplates.

Exploring the mechanical performance of structures resting on EF, most researchers tend to utilize either Winkler foundation Winkler (1867) or Pasternak foundation Pasternak (1954). For example, Fazzolari (2018) used an ES to analyze the buckling of FGP beams. Xiang et al. (1994) also used an ES for the free vibration analysis of Mindlin plates. Omurtag et al. (1997) based on FEM to study the free vibration of the Kirchhoff plates. Matsunaga (2000) employed an ES based on HSDT to study the buckling of plates. Thai and Kim (2013) calculated the buckling of FGM plates by using an ES based on third-order shear deformation theory (TSDT) and so on.

To enhance the convergence and precision of traditional triangular elements, researchers have integrated the original mixed interpolation of the tensorial components technique for the three-node triangular element (MITC3) Lee and Bathe (2004) with the edge-based smoothed finite element method (ES-FEM) Liu et al. (2009), resulting in the newly introduced ES-MITC3 (Chau-Dinh et al. 2017; Pham et al. 2018; Pham et al. 2020; Pham-Tien et al. 2018; Nguyen-Thoi 2020). The outcomes of our current investigation illustrate that the ES-MITC3 exhibits the following notable advantages:

Buckling analysis of functionally graded porous variable thickness plates resting on Pasternak foundation
using ES-MITC3

Truong Thanh Nguyen et al.

(1) The ES-MITC3 effectively mitigates the occurrence of transverse shear locking, even when the thickness-to-length ratio of the structures reaches as low as 10^{-8} Chau-Dinh et al. (2017); (2) The ES-MITC3 exhibits superior accuracy when compared to conventional triangular element.

Through analysis of the above documents, it can be seen that it can be seen that previous studies on buckling of structures mainly used analytical methods and classical FEM with constant thickness. Therefore, the achieved results are limited by the complex geometric model and boundary conditions. In addition, there has been no prior investigation into the buckling of FGP VT plates located on a PF using the ES-MITC3. This is what motivates us to do this work. To validate the accuracy and reliability of the proposed method, we thoroughly compare our numerical findings with those derived from existing methodologies. Then, this study delves into the comprehensive exploration of the impact of input parameters on the buckling of FGP VT plates. The obtained results are expected to contribute to the general understanding of the buckling of FGP VT plates.

2 THEORETICAL FORMULATION

2.1 FGP material

The mechanical properties of FGP plates following the rule of mixed are defined by Chen et al. (2015):

$$P(z) = [(P_c - P_m)V_c(z) + P_m]\left[1 - \Omega\cos\left(\frac{\pi z}{h(x,y)}\right)\right] \tag{1a}$$

with

$$V_c(z) = \left(\frac{z}{h(x,y)} + 0.5\right)^p \text{ with } z \in \left(-\frac{h(x,y)}{2}; \frac{h(x,y)}{2}\right) \tag{1b}$$

where $P(z)$ stands for elastic modulus $E(z)$, Poisson's ratio $v(z)$; symbols m and c represent the metal and ceramic constituents; $V_c(z)$ is the volume fraction of ceramic; p is the power-law index; and Ω denotes the maximum porosity value.

2.2 Pasternak foundation

In this study, the FGP plate resting on EF following Pasternak's model is determined by Pasternak (1954):

$$\mathcal{R} = k_1 w(x,y) - k_2\left[\left(\frac{\partial w}{\partial x}\right)^2 + \left(\frac{\partial w}{\partial y}\right)^2\right] \tag{2}$$

with k_1 is springer stiffness and k_2 is shear stiffness. The negative sign in front of the second term indicates that the shear resistance is opposite to the direction of curvature. This means that when the deflection is concave upward, the shear resistance is downward, and vice versa. The negative sign also ensures that the total foundation reaction is zero when there is no deflection.

2.3 Mindlin plate theory

In accordance with FSDT, the displacement field of FGP plates is expressed by Ramu and Mohanty (2014):

$$\begin{cases} u(x,y,z) = u_0(x,y) + z\theta_x(x,y) \\ v(x,y,z) = v_0(x,y) + z\theta_y(x,y) \\ w(x,y,z) = w_0(x,y) \end{cases} \tag{3}$$

in which $u, v, w, \theta_x, \theta_y$ are unknown displacements.

The strain field is defined by

$$\boldsymbol{\varepsilon} = \begin{Bmatrix} \varepsilon_x \\ \varepsilon_y \\ \varepsilon_{xy} \\ \gamma_{xz} \\ \gamma_{yz} \end{Bmatrix} = \begin{Bmatrix} u_{,x} \\ v_{,y} \\ u_{,y} + v_{,x} \\ w_{,x} + u_{,z} \\ w_{,y} + v_{,z} \end{Bmatrix} = \begin{Bmatrix} u_{0,x} \\ v_{0,y} \\ u_{0,y} + v_{0,x} \\ v_{0,x} + \theta_x \\ w_{0,y} + \theta_y \end{Bmatrix} + z\begin{Bmatrix} \theta_{x,x} \\ \theta_{y,y} \\ \theta_{x,y} + \theta_{y,x} \\ 0 \\ 0 \end{Bmatrix}; \tag{4}$$

Buckling analysis of functionally graded porous variable thickness plates resting on Pasternak foundation
using ES-MITC3

Truong Thanh Nguyen et al.

Eq. (4) may be re-written by

$$\boldsymbol{\varepsilon} = \begin{Bmatrix} \boldsymbol{\varepsilon}_1 \\ \boldsymbol{\varepsilon}_2 \end{Bmatrix} = \begin{Bmatrix} \boldsymbol{\varepsilon}_m + z\boldsymbol{\kappa} \\ \boldsymbol{\gamma} \end{Bmatrix}; \tag{5}$$

The stress-strain relations are determined following Hooke's law as follows:

$$\begin{Bmatrix} \sigma_x \\ \sigma_y \\ \sigma_{xy} \\ \tau_{xz} \\ \tau_{yz} \end{Bmatrix} = \begin{bmatrix} Q_{11} & Q_{12} & 0 & 0 & 0 \\ Q_{21} & Q_{22} & 0 & 0 & 0 \\ 0 & 0 & Q_{66} & 0 & 0 \\ 0 & 0 & 0 & Q_{55} & 0 \\ 0 & 0 & 0 & 0 & Q_{44} \end{bmatrix} \begin{Bmatrix} \varepsilon_x \\ \varepsilon_y \\ \varepsilon_{xy} \\ \gamma_{xz} \\ \gamma_{yz} \end{Bmatrix} \tag{6}$$

in which

$$Q_{11} = Q_{22} = \frac{E(z)}{1-\nu(z)^2}; Q_{12} = Q_{21} = \frac{\nu(z)E(z)}{1-\nu(z)^2};$$

$$Q_{44} = Q_{55} = Q_{66} = \frac{E(z)}{2(1+\nu(z))}. \tag{7}$$

The force and moment resultants are defined by:

$$\{N_x \ N_y \ N_{xy}\}^T = \boldsymbol{A}\boldsymbol{\varepsilon}_m + \boldsymbol{B}\boldsymbol{\kappa}; \tag{8a}$$

$$\{M_x \ M_y \ M_{xy}\}^T = \boldsymbol{B}\boldsymbol{\varepsilon}_m + \boldsymbol{C}\boldsymbol{\kappa}; \tag{8b}$$

$$\{Q_{xz} \quad Q_{yz}\}^T = \boldsymbol{A}^s\boldsymbol{\gamma}. \tag{8c}$$

with

$$(\boldsymbol{A}, \boldsymbol{B}, \boldsymbol{C}) = \int_{-h(x,y)/2}^{h(x,y)/2} \begin{bmatrix} Q_{11} & Q_{12} & 0 \\ Q_{21} & Q_{22} & 0 \\ 0 & 0 & Q_{66} \end{bmatrix} (1, z, z^2) dz \, ; \, \boldsymbol{A}^s = \int_{-h(x,y)/2}^{h(x,y)/2} \begin{bmatrix} Q_{55} & 0 \\ 0 & Q_{44} \end{bmatrix} dz. \tag{9}$$

Note that, all the matrices in Eq. (9) are influenced by the thickness variation profile. As a result, the integration limits are contingent upon the specific positions of points across the plate.

2.4 Finite element formulation

The generalized displacements at any point $\boldsymbol{u}^e = \left[u_j^e, v_j^e, w_j^e, \theta_{xj}^e, \theta_{yj}^e\right]^T$ of the element ψ_e is defined by Lee and Bathe (2004):

$$\boldsymbol{u}^e(\boldsymbol{x}) = \sum_{j=1}^{n^{ne}} \begin{bmatrix} N_I(x) & 0 & 0 & 0 & 0 \\ 0 & N_I(x) & 0 & 0 & 0 \\ 0 & 0 & N_I(x) & 0 & 0 \\ 0 & 0 & 0 & N_I(x) & 0 \\ 0 & 0 & 0 & 0 & N_I(x) \end{bmatrix} \boldsymbol{d}_j^e = \sum_{j=1}^{n^{ne}} \boldsymbol{N}(x) \boldsymbol{d}_j^e \tag{10}$$

where n^{ne} is the total of nodes; $\boldsymbol{N}(\boldsymbol{x})$ is the shape function matrix; and $\boldsymbol{d}_j^e = \left[u_j^e, v_j^e, w_j^e, \theta_{xj}^e, \theta_{yj}^e\right]^T$ are the nodal-DOF associated with the jth node of ψ_e.

Buckling analysis of functionally graded porous variable thickness plates resting on Pasternak foundation using ES-MITC3

Truong Thanh Nguyen et al.

The membrane bending strains of MITC3 by Lee and Bathe (2004) is:

$$\boldsymbol{\varepsilon}_m^e = [\boldsymbol{B}_{m1}^e \quad \boldsymbol{B}_{m2}^e \quad \boldsymbol{B}_{m3}^e] \boldsymbol{d}^e = \boldsymbol{B}_m^e \, \boldsymbol{d}^e \tag{11a}$$

$$\boldsymbol{\kappa}^e = [\boldsymbol{B}_{b1}^e \quad \boldsymbol{B}_{b2}^e \quad \boldsymbol{B}_{b3}^e] \boldsymbol{d}^e = \boldsymbol{B}_b^e \, \boldsymbol{d}^e \tag{11b}$$

The smoothing domains ψ^k is established based on the edges of Q3 such that $\psi = \bigcup_{k=1}^{n^k} \psi^k$ and $\psi_i^k \cap \psi_j^k = \emptyset$ for $i \neq j$. An edge-based smoothing domain ψ^k for the inner edge k is formed by connecting two end-nodes of the edge to the centroids of adjacent MITC3 as shown in Fig 1.
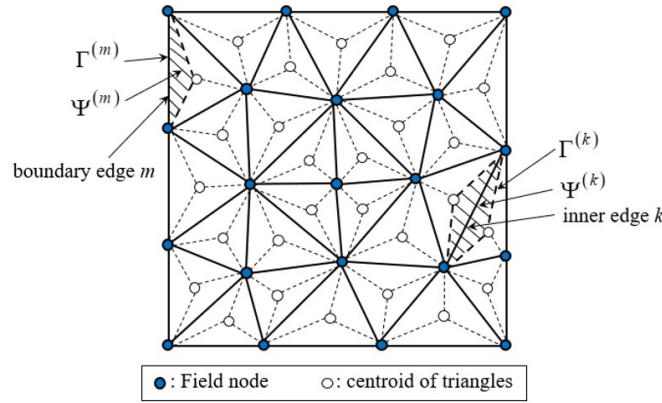

Figure 1 The smoothing domain ψ^k.

Using the edge-based smooth technique by Liu et al. (2009), the smoothed membrane, bending and shear strains $\tilde{\boldsymbol{\varepsilon}}_m^k, \tilde{\boldsymbol{\kappa}}^k, \tilde{\boldsymbol{\gamma}}^k$ can be defined by

$$\tilde{\boldsymbol{\varepsilon}}_m^k = \int_{\psi^k} \boldsymbol{\varepsilon}_m \, \Phi^k(\mathrm{x}) \mathrm{d}\psi, \tag{12a}$$

$$\tilde{\boldsymbol{\kappa}}^k = \int_{\psi^k} \boldsymbol{\kappa} \, \Phi^k(\mathrm{x}) \mathrm{d}\psi, \tag{12b}$$

$$\tilde{\boldsymbol{\gamma}}^k = \int_{\psi^k} \boldsymbol{\gamma} \, \Phi^k(\mathrm{x}) \mathrm{d}\psi, \tag{12c}$$

where $\Phi^k(\mathrm{x})$ is a smoothing function with $\int_{\psi^k} \Phi^k(\mathrm{x}) \mathrm{d}\psi = 1$.

In this article, the constant smoothing function is used Liu et al. (2009):

$$\Phi^k(\mathrm{x}) = \begin{cases} \frac{1}{A^k} \; \mathrm{x} \in \psi^k \\ 0 \; \mathrm{x} \notin \psi^k \end{cases} \tag{13}$$

with A^k is the area of the smoothing domain ψ^k.

Now, the stiffness matrix of the FGP plate is determined by Liu et al. (2009):

$$\tilde{\mathbf{K}}_p = \sum_{k=1}^{n_{sh}^k} \tilde{\mathbf{K}}_e^k \tag{14}$$

where $\tilde{\mathbf{K}}_e^k$ is defined by

$$\tilde{K}_e^k = \int_{\psi^k} \left(\tilde{\boldsymbol{B}}^{kT} \begin{bmatrix} \boldsymbol{A} & \boldsymbol{B} \\ \boldsymbol{B} & \boldsymbol{C} \end{bmatrix} \tilde{\boldsymbol{B}}^k + \tilde{\boldsymbol{B}}_s^{kT} \boldsymbol{A}^s \tilde{\boldsymbol{B}}_s^k \right) d\psi = \tilde{\boldsymbol{B}}^{kT} \begin{bmatrix} \boldsymbol{A} & \boldsymbol{B} \\ \boldsymbol{B} & \boldsymbol{C} \end{bmatrix} \tilde{\boldsymbol{B}}^k A^k + \tilde{\boldsymbol{B}}_s^{kT} \boldsymbol{A}^s \tilde{\boldsymbol{B}}_s^k A^k \tag{15}$$

Buckling analysis of functionally graded porous variable thickness plates resting on Pasternak foundation
using ES-MITC3

Truong Thanh Nguyen et al.

in which the strain-displacement matrix $\widetilde{\boldsymbol{B}}^{kT}$ is determined by Nguyen-Thoi (2020):

$$\widetilde{\boldsymbol{B}}^{kT} = \begin{bmatrix} \widetilde{\boldsymbol{B}}^k_{mj} & \widetilde{\boldsymbol{B}}^k_{bj} \end{bmatrix} \tag{16}$$

The geometric stiffness matrix of the FGP plate is determined by Pham et al. (2020):

$$\widetilde{\mathbf{K}}_g = \sum_{k=1}^{n^k_{sh}} \widetilde{\mathbf{K}}_g^{ek} \text{ with } \widetilde{\mathbf{K}}_g^e = \int_{\psi^k} \left(\widetilde{\boldsymbol{Y}}_i^T \overline{\boldsymbol{N}} \widetilde{\boldsymbol{Y}}_i \right) d\psi \tag{17}$$

where

$$\overline{\boldsymbol{N}} = \begin{bmatrix} \overline{N}_x & \overline{N}_{xy} \\ \overline{N}_{xy} & \overline{N}_y \end{bmatrix} \tag{18}$$

with

$$(\overline{N}_x, \overline{N}_y, \overline{N}_{xy}) = \int_{-h(x,y)}^{h(x,y)} (\sigma_x, \sigma_y, \sigma_{xy}) dz \tag{19}$$

and $\widetilde{\boldsymbol{Y}}_i$ is presented by Pham et al. (2020). Note that, Eq. (19) is integrated as Eq. (9).

The stiffness foundation matrix is determined by Nguyen-Thoi (2020):

$$\boldsymbol{K}_f = \sum_{k=1}^{n^k} \boldsymbol{K}_f^e \tag{20a}$$

with

$$\boldsymbol{K}_f^e = k_1 \int_{\psi_e} \mathbf{N}_w^T \mathbf{N}_w \, d\psi_e + k_2 \int_{\psi_e} \left[\left(\frac{\partial \mathbf{N}_w}{\partial x} \right)^T \left(\frac{\partial \mathbf{N}_w}{\partial x} \right) + \left(\frac{\partial \mathbf{N}_w}{\partial y} \right)^T \left(\frac{\partial \mathbf{N}_w}{\partial y} \right) \right] d\psi_e \tag{20b}$$

Apply the principle of minimum total potential energy, the equation to determine the critical force P_{cr} as follows:

$$\left| \left(\widetilde{\mathbf{K}}_p + \boldsymbol{K}_f \right) + P_{cr} \widetilde{\mathbf{K}}_g \right| = 0 \tag{21}$$

The BCs in this study are defined by

Simply supported (S):

$$u_0 = w = \varphi_x = 0 \text{ at } y = 0, y = b \text{ or } v_0 = w = \varphi_y = 0 \text{ at } x = 0, x = a$$

Clamped (C):

$$u_0 = w = \varphi_x = \varphi_y = 0 \text{ at } y = 0, y = b \text{ or } v_0 = w = \varphi_x = \varphi_y = 0 \text{ at } x = 0, x = a.$$

3. Verification

To facilitate the numerical survey process, the dimensionless formulas are introduced by

$$P_{cri}^* = \frac{P_{cri} a^2}{E_m h^3}; K_1 = \frac{k_1 a^4}{D}; \ K_2 = \frac{k_2 a^2}{D} \text{ with } D = \frac{E_m h^3}{12(1-v_m^2)} \tag{22}$$

and the mechanical properties of FGP plates are listed in Table 1.

Buckling analysis of functionally graded porous variable thickness plates resting on Pasternak foundation using ES-MITC3

Truong Thanh Nguyen et al.

Table 1 The mechanical properties of component materials.

Materials	Elastic modulus (GPa)	Mass density (kg/m³)	Poisson's ratio
Al_2O_3	380	3800	0.3
Al	70	2707	0.3

Firstly, consider the SSSS FGM (Al/Al_2O_3) constant-thickness plate with material properties as shown in Table 1. The obtained dimensionless critical load P_{cr}^* of FGM plates are shown in Table 2. It can be observed that the results of the ES-MITC3 converge at the mesh size of 18×18 and are close to those of Thai and Kim (2013). The error in the results comes from the fact that we use FEM based on FSDT while Thai and Kim (2013) used an exact solution based on TSDT. Additionally, the value of the obtained results is smaller than those of their study. From here, we will use a mesh size of 18×18 for the next examples.

Secondly, let us consider the SSSS isotropic VT plate with $h = h_0(1 + \alpha\frac{y}{b})$. The dimensionless critical load is given by $P_{cr}^{**} = 12P_{cr}b^2/(\pi^2 Eh_0^3)$ and listed in Table 3. It can be seen that the gained results are in good agreement with those of Banh-Thien et al. (2017) using the first-order IGA and Eisenberger and Alexandrov (2003) employed the Kantorovich method. The obtained results also show the effectiveness of the proposed method compared to the state-of-the-art numerical method (IGA). From the above two examples, the accuracy and performance of the proposed method can be confirmed.

Table 2 The convergence of critical load of SSSS square FGM plates ($\Omega = 0$).

(K_1, K_2)	Method	Mesh size	p					
			0	0.5	1	2	5	10
(0,0)	Present	12×12	16.9775	11.571	9.4069	7.6759	6.2244	5.324
		14×14	16.9579	11.5545	9.3907	7.6608	6.2132	5.3161
		16×16	16.946	11.5443	9.3805	7.6512	6.2061	5.3112
		18×18	16.9381	11.5375	9.3737	7.6447	6.2013	5.3080
		20×20	16.9381	11.5375	9.3737	7.6447	6.2013	5.3080
	Thai and Kim (2013)		18.5785	12.1229	9.3391	7.2631	6.0353	5.4528
(100,10)	Present	12×12	19.1946	13.789	11.5857	9.7572	8.2014	7.3051
		14×14	19.1799	13.777	11.5729	9.7426	8.1897	7.2988
		16×16	19.1711	13.7697	11.565	9.7333	8.1823	7.2949
		18×18	19.1655	13.765	11.5597	9.727	8.1772	7.2924
		20×20	19.1655	13.765	11.5597	9.727	8.1772	7.2924
	Thai and Kim (2013)		21.3379	14.8823	12.0985	10.0224	8.7947	8.2122

Table 3 Comparison of critical load of SSSS VT plates.

α	a/b								
	0.5			0.7			0.9		
	Eisenberger and Alexandrov (2003)	Banh-Thien et al. (2017)	Present	Eisenberger and Alexandrov (2003)	Banh-Thien et al. (2017)	Present	Eisenberger and Alexandrov (2003)	Banh-Thien et al. (2017)	Present
0.125	7.4645	7.4621	7.4625	5.4199	5.4194	5.4198	4.8413	4.8428	4.8418
0.25	8.7633	8.7531	8.7601	6.3891	6.3869	6.3885	5.7165	5.7224	5.7203
0.5	11.6112	11.5687	11.5989	8.5741	8.5627	8.5738	7.7111	7.7327	7.7198
0.75	14.7942	14.6953	16.6987	11.0979	11.0657	11.0889	10.046	10.0858	10.0683
1	18.3175	18.1368	18.2981	13.973	13.9017	13.9865	12.7381	12.7877	12.7524

4 NUMERICAL RESULTS AND DISCUSSION

4.1 Buckling analysis of FGP plate with linear variable-thickness in both x-, y- directions

In this section, let us consider an FGP plate with linear VT in both x-, y- directions in the coordinate system as shown in Fig .2a.

Buckling analysis of functionally graded porous variable thickness plates resting on Pasternak foundation
using ES-MITC3

Truong Thanh Nguyen et al.

a) Linear VT in both x-, y- directions
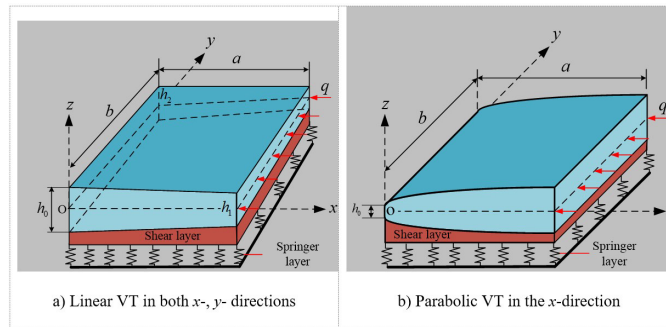
b) Parabolic VT in the x-direction

Figure 2 The model of the FGP with different rules of VT.

Firstly, Fig. 3 presents the first six buckling mode shapes of the SSSS FGP ($h_0 = a/45$, $h_1 = h_2 = a/65$, a is fixed) with thickness varies both the x- and y-direction: $h(x) = h_1 + \frac{h_0 - h_1}{a}(a - x), h(y) = h_2 + \frac{h_0 - h_2}{b}(b - y)$, respectively. The remaining parameters are $p = 1, \Omega = 0.1, K_1 = 100,$ and $K_2 = 10$. It can be observed that the mode shape of the FGP plate is not symmetrical due to the non-uniform thickness of the plate. The maximum deflection values of the mode shape travel to the position of a smaller thickness.
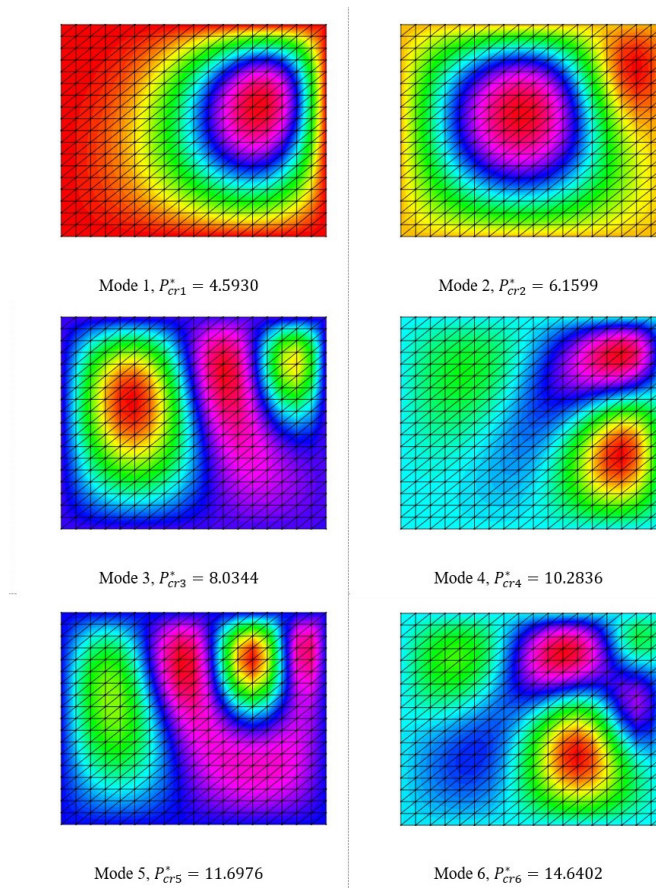

Mode 1, $P_{cr1}^* = 4.5930$

Mode 2, $P_{cr2}^* = 6.1599$

Mode 3, $P_{cr3}^* = 8.0344$

Mode 4, $P_{cr4}^* = 10.2836$

Mode 5, $P_{cr5}^* = 11.6976$

Mode 6, $P_{cr6}^* = 14.6402$

Figure 3 The first six buckling mode shapes of the SSSS VT FGP plate (top view).

Secondly, the simultaneous influence of foundation stiffness (K_1, K_2) on the critical load of the CCCC FGP VT plate is displayed in Fig. 4 and Table 4. In this study, the a/b ratio gets values $a/b = 0.5, 1, 1.5, 2$ with remaining parameters as $h_0 = a/50$, $h_1 = h_2 = a/75, p = 0.5,$ and $\Omega = 0.5$. It can be seen that the foundation increases the FGP plate stiffness, thus making the dimensionless critical load larger. Moreover, the figures also indicate that the shear layer provides better support than the spring layer. Besides, with the same material parameters and BCs, the FGP plate with smaller areas will be stiffer resulting in a higher critical load corresponding to $a/b = 2, 1.5, 1, 0.5,$ as expected.
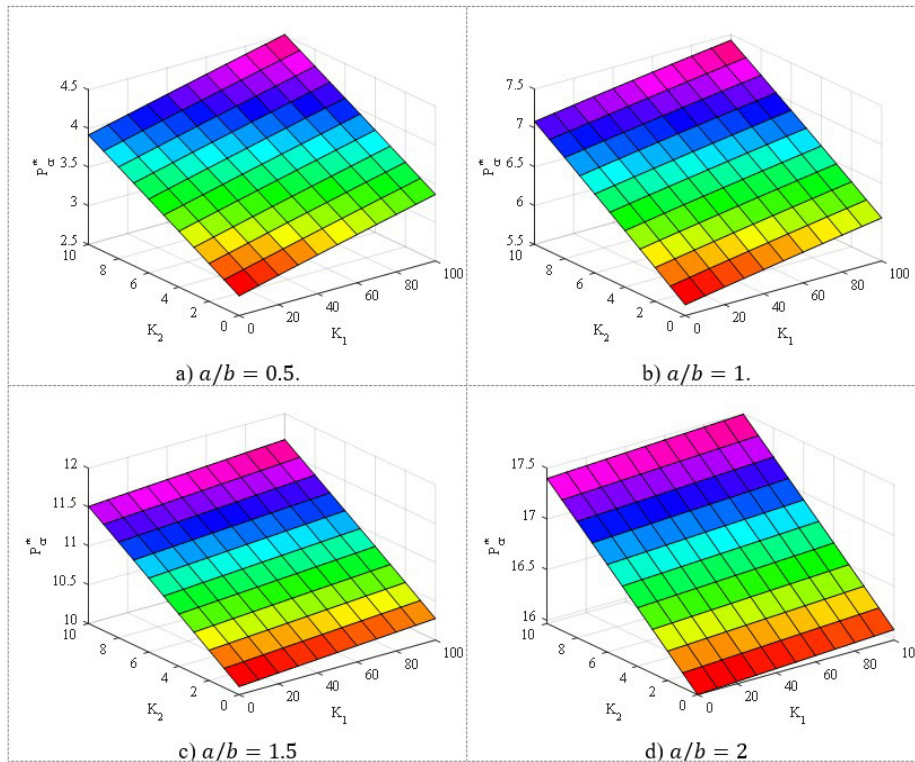
Buckling analysis of functionally graded porous variable thickness plates resting on Pasternak foundation
using ES-MITC3

Truong Thanh Nguyen et al.

Figure 4 The simultaneous effect of foundation stiffness (K_1, K_2) on the critical load of FGP VT plates.

Table 4 The critical load of the CCCC FGP VT rectangular plate.

a/b	K_1	K_2					
		0	2	4	6	8	10
0.5	0	2.7548	2.9898	3.2232	3.4552	3.686	3.9156
	20	2.8792	3.1138	3.3468	3.5785	3.8088	4.038
	40	3.0022	3.2363	3.4689	3.7001	3.9301	4.1588
	60	3.1235	3.3572	3.5894	3.8201	4.0496	4.2779
	80	3.2430	3.4763	3.708	3.9384	4.1674	4.3952
	100	3.3608	3.5936	3.8248	4.0547	4.2832	4.5105
1	0	5.6378	5.9344	6.2269	6.5154	6.800	7.0808
	20	5.7255	6.0193	6.309	6.5947	6.8765	7.1545
	40	5.8109	6.1018	6.3888	6.6717	6.9507	7.2259
	60	5.8939	6.1821	6.4662	6.7463	7.0226	7.2951
	80	5.9746	6.26	6.5413	6.8186	7.0922	7.3621
	100	6.0530	6.3355	6.6140	6.8887	7.1596	7.4269
1.5	0	10.1041	10.3888	10.6714	10.9519	11.2305	11.5073
	20	10.1392	10.4233	10.7052	10.9852	11.2632	11.5395
	40	10.1741	10.4575	10.7388	11.0182	11.2957	11.5715
	60	10.2087	10.4915	10.7722	11.0511	11.328	11.6033
	80	10.2431	10.5253	10.8055	11.0837	11.3602	11.6349
	100	10.2773	10.5589	10.8385	11.1162	11.3921	11.6664
2	0	15.9689	16.2580	16.5454	16.8311	17.1153	17.3981
	20	15.9896	16.2783	16.5654	16.8509	17.1349	17.4174
	40	16.0101	16.2986	16.5855	16.8707	17.1544	17.4366
	60	16.0307	16.3189	16.6054	16.8904	17.1739	17.4558
	80	16.0511	16.3391	16.6254	16.9101	17.1933	17.4750
	100	16.0716	16.3592	16.6452	16.9297	17.2126	17.4941

Buckling analysis of functionally graded porous variable thickness plates resting on Pasternak foundation
using ES-MITC3

Truong Thanh Nguyen et al.

Thirdly, the effect of material parameters (p, Ω) on critical load of the SCSC FGP variable thickness square plate with parameters $a/b = 1$, $h_0 = a/30$, $h_1 = h_2 = a/45$, $K_1 = 50$, and $K_2 = 5$ is presented in Fig. 5. Observing that the critical load of the FGP plate depends on both the power-law index p and the maximum porosity Ω. Specifically, the ceramic-rich plate will be harder, leading to a larger critical load. Moreover, the critical load decreases rapidly in the (0-2) range and changes little when p is greater than 2. Besides, the pores reduce the plate stiffness thereby reducing the critical load, as expected. In addition, Table 5 further lists the first six critical loads of square FGP VT square plates with input parameters: $a/b = 1$, $h_0 = a/25$, $h_1 = h_2 = a/40$, $K_1 = 75$, and $K_2 = 15$.

a) The effect of p on the critical load.

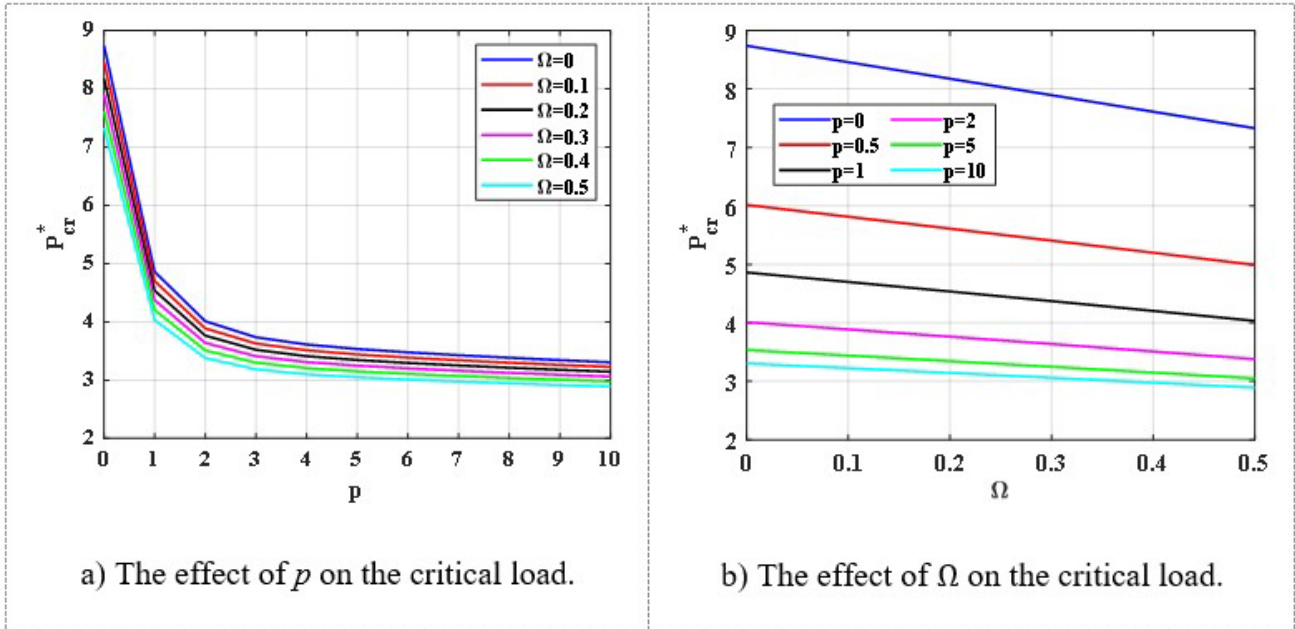b) The effect of Ω on the critical load.

Figure 5 The effect of material parameters on buckling of the SCSC FGP VT square plate.

Table 5 The first six critical load of square FGP VT square plates.

Critical load	P_{cr1}^*	P_{cr2}^*	P_{cr3}^*	P_{cr4}^*	P_{cr5}^*	P_{cr6}^*
BCs			SSSS			
$\Omega = 0, p = 0$	5.7044	7.9811	10.0891	12.904	13.7395	17.9827
$\Omega = 0.1, p = 1$	3.7483	5.0558	6.0108	7.1815	7.5182	9.5504
$\Omega = 0.2, p = 2$	3.2508	4.2839	5.1417	5.8262	6.0967	7.5113
$\Omega = 0.3, p = 4.5$	3.0356	3.934	4.7652	5.2638	5.4955	6.6151
$\Omega = 0.5, p = 9.5$	2.7715	3.495	4.2488	4.6364	4.7871	5.5411
BCs			SCSC			
$\Omega = 0, p = 0$	9.9597	11.6684	16.527	19.5379	21.8406	25.4488
$\Omega = 0.1, p = 1.5$	5.2514	5.9171	7.9955	9.0897	10.2156	11.6418
$\Omega = 0.3, p = 2$	4.6811	5.2336	6.9822	7.8401	8.8388	9.976
$\Omega = 0.4, p = 4.5$	4.1672	4.6184	6.0655	6.7179	7.6034	8.4581
$\Omega = 0.5, p = 9$	3.8733	4.2656	5.5366	6.0815	6.8982	7.5818

4.2 Buckling analysis of FGP plate with parabolic variable thickness in x-direction

In this study, an FGP parabolic VT plate with $h = h(x) = h_0 \left[1 + \left(\frac{x}{a} \right)^2 \right]$ in x-direction is considered (see Fig. 2b).

Firstly, Fig. 6 shows the first six buckling mode shapes of the SSSS FGP VT plate ($h_0 = a/25$ a is fixed). The remaining parameters are $p = 0.5$, $\Omega = 0.3$, $K_1 = 50$, and $K_2 = 10$. It can be seen that the mode shape of the FGP VT plate is deflected to the left in the x-direction, as expected.
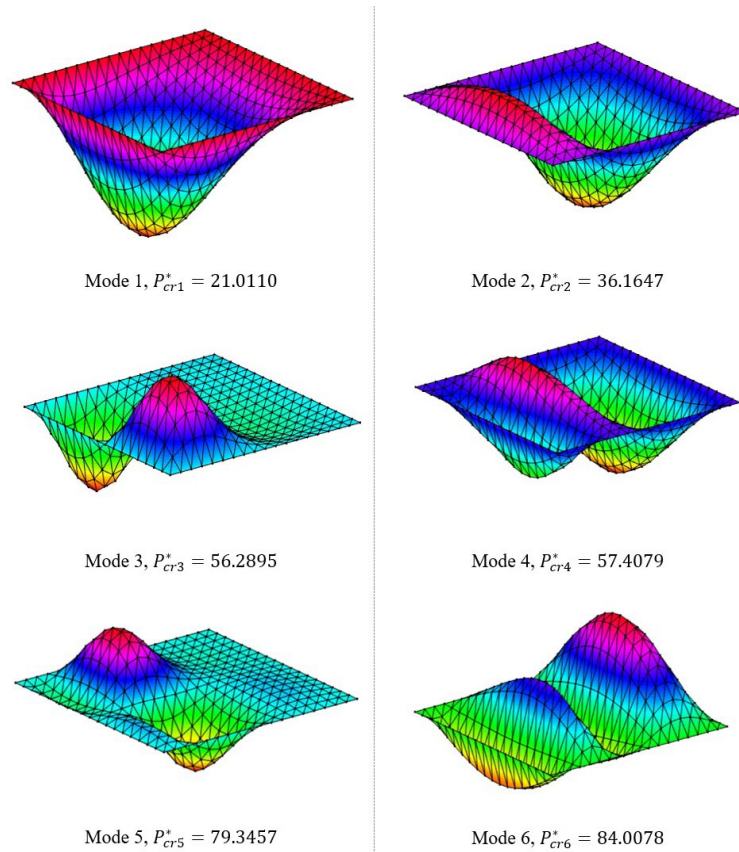
Buckling analysis of functionally graded porous variable thickness plates resting on Pasternak foundation using ES-MITC3

Truong Thanh Nguyen et al.

Mode 1, $P^*_{cr1} = 21.0110$

Mode 2, $P^*_{cr2} = 36.1647$

Mode 3, $P^*_{cr3} = 56.2895$

Mode 4, $P^*_{cr4} = 57.4079$

Mode 5, $P^*_{cr5} = 79.3457$

Mode 6, $P^*_{cr6} = 84.0078$

Figure 6 The first six buckling mode shapes of the FGP VT square plate.

Secondly, the simultaneous effect of material parameters (p, Ω) on the buckling of the SCSC VT FGP rectangular plate is displayed in Fig. 7 and Table 6. In this study, the remaining parameters as $h_0 = a/60, h_1 = a/75, K_1 = 75, and K_2 = 15$, and the a/b ratio takes values $0.5, 1, 1.5, 2$. It can be seen that the increase in p and/or Ω reduces the critical load of the FGP plate, as expected. Besides, the impact of p on the critical load is more pronounced than that of Ω.

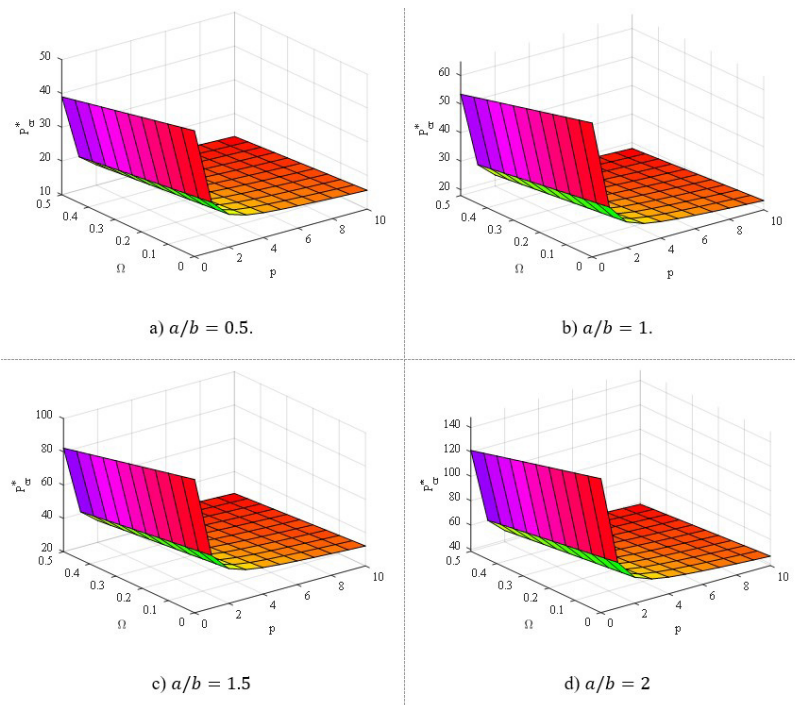

a) $a/b = 0.5$.

b) $a/b = 1$.

c) $a/b = 1.5$

d) $a/b = 2$

Figure 7 The simultaneous effect of foundation stiffness (p, Ω) on the buckling of FGP VT plates.

Table 6 The critical load of the SCSC FGP VT rectangular plate.

a/b	p	Ω					
		0	0.1	0.2	0.3	0.4	0.5
0.5	0	47.2858	45.6364	43.9859	42.3341	40.6807	39.0252
	2	19.6898	18.9784	18.2596	17.5319	16.7933	16.0408
	4	17.3742	16.8009	16.2219	15.6363	15.0427	14.4392
	6	16.5914	16.0688	15.5411	15.0072	14.466	13.9159
	8	16.0368	15.5492	15.0567	14.5582	14.0527	13.5386
	10	15.5678	15.1083	14.6439	14.1739	13.6971	13.2121
1	0	64.8525	62.5773	60.3002	58.0208	55.7386	53.4527
	2	26.8777	25.8967	24.9055	23.9019	22.8831	21.8451
	4	23.681	22.8905	22.0922	21.2846	20.4658	19.6334
	6	22.5982	21.8777	21.15	20.4138	19.6673	18.9085
	8	21.8324	21.16	20.4807	19.7931	19.0957	18.3864
	10	21.1858	20.5519	19.9114	19.2629	18.6049	17.9355
1.5	0	100.1082	96.5418	92.9711	89.3954	85.8132	82.2227
	2	40.9157	39.3794	37.8269	36.2547	34.6582	33.0315
	4	35.8961	34.6584	33.4083	32.1436	30.861	29.5569
	6	34.1879	33.0599	31.9204	30.7674	29.5981	28.4093
	8	32.9838	31.9309	30.8668	29.7897	28.6969	27.5852
	10	31.9712	30.9781	29.9743	28.9578	27.9263	26.8765
2	0	148.3186	142.931	137.5344	132.1266	126.7048	121.2653
	2	59.736	57.4212	55.082	52.713	50.3075	47.8563
	4	52.1433	50.2806	48.3993	46.4959	44.5657	42.6032
	6	49.5414	47.8446	46.1305	44.3961	42.6373	40.8491
	8	47.7169	46.1328	44.532	42.9115	41.2675	39.5951
	10	46.1918	44.6971	43.1862	41.6563	40.1037	38.5236

Thirdly, the effect of foundation stiffness (K_1, K_2) on critical load of the SSSS VT FGP square plate with parameters $a/b = 1, h_0 = a/45, h_1 = a/60, p = 4,$ and $\Omega = 0.4$ is shown in Fig. 8. Observing that the supporting foundation makes the plate stiffer leading to the expected increase in critical load. In addition, the influence of the shear layer on critical loads is greater than that of the springer layer, as expected. Besides, Table 7 further gives the first six critical loads of square FGP VT square plates with input parameters: $a/b = 1, h_0 = a/55, p = 10,$ and $\Omega = 0.2$.
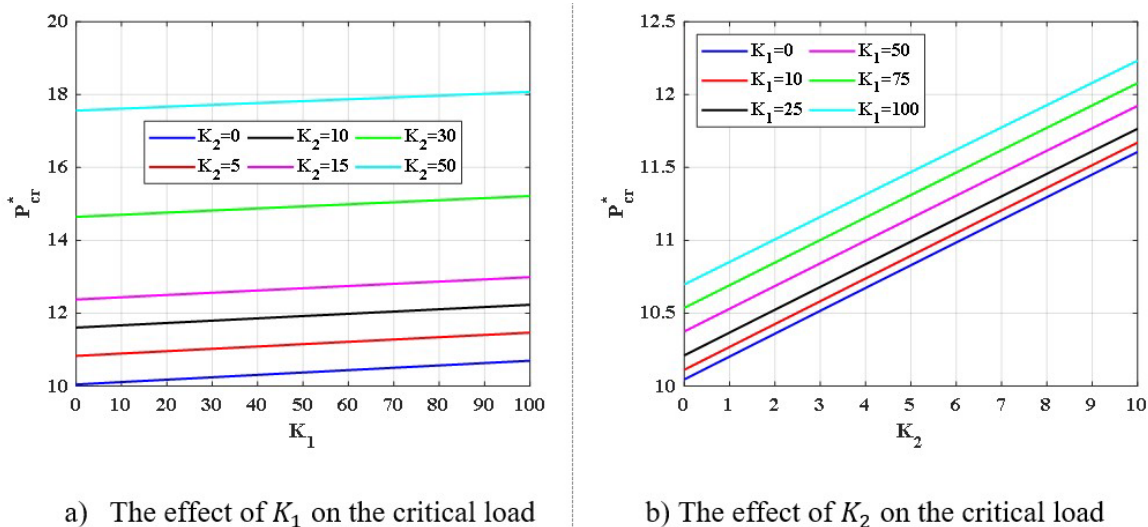

a) The effect of K_1 on the critical load

b) The effect of K_2 on the critical load

Figure 8 The effect of foundation stiffness on buckling of the SCSC FGP VT plate.

Buckling analysis of functionally graded porous variable thickness plates resting on Pasternak foundation
using ES-MITC3

Truong Thanh Nguyen et al.

Table 7 The first six critical load of square FGP VT plates.

Critical load	P_{cr1}^*	P_{cr2}^*	P_{cr3}^*	P_{cr4}^*	P_{cr5}^*	P_{cr6}^*
BCs			SSSS			
$K_1 = 0, K_2 = 0$	2.4207	3.9295	6.7648	8.7439	10.8023	12.1352
$K_1 = 100, K_2 = 0$	3.2084	4.2674	6.8709	8.9505	10.8642	12.2871
$K_1 = 0, K_2 = 10$	4.1183	5.189	7.7973	10.4311	11.8079	13.6353
$K_1 = 100, K_2 = 10$	4.7254	5.7008	7.9049	10.6085	11.8695	13.7809
			CCCC			
$K_1 = 0, K_2 = 0$	6.0813	7.2696	11.9995	14.7977	16.1446	17.0154
$K_1 = 50, K_2 = 0$	6.343	7.3816	12.1214	14.8735	16.1884	17.069
$K_1 = 0, K_2 = 5$	6.8505	7.8589	12.6061	15.5793	16.7132	17.6719
$K_1 = 50, K_2 = 5$	7.0922	7.9795	12.736	15.6514	16.7551	17.7265

5. Conclusion

The primary objective of this study is to enhance the applicability of ES-MITC3 in the analysis of buckling behaviour for FGP VT plates supported by the Pasternak foundation. This combination of the FSDT and ES-MITC3 is chosen for its simplicity and performance. The work also presents the influence of parameters such as geometric dimensions, material properties, boundary conditions and changes in thickness rules on the buckling behaviour of FGP plates. The formulation and subsequent numerical findings lead to several key conclusions as outlined below:

- ES-MITC3 is based on classical triangular elements, so it is easy to mesh elements even with complex geometries.

- The increase of power-law index p and/or Ω leads to the reduction of the FGP plate stiffness, thereby reducing the critical load. Besides, the influence of p on the buckling of FGP plates is more significant than Ω.

- The elastic foundation increases the FGP plate stiffness, leading to an increase in the critical load, as expected. Furthermore, the influence of shear stiffness K_2 on the critical load is larger than the influence of springer stiffness K_1.

- The ES-MITC3, when applied in conjunction with the FSDT, is best suited for the analysis of thin to medium-thickness plates. In cases involving thick plates, it is advisable to pair the ES-MITC3 element with the HSDT for more accurate results.

- The numerical results obtained from this study are anticipated to provide valuable insights for the calculation and design of FGP VT plates in practical engineering applications.

Author's Contributions: Methodology, Validation, Formal analysis, Investigation, Writing Original draft, Truong Thanh Nguyen; Software, Validation, Investigation, Visualization, Writing Original draft, Truong Son Le and Trung Thanh Tran; Conceptualization, Writing - Reviewing & Editing, Supervision, Project administration, Quoc-Hoa Pham.

Editor: Marco L. Bittencourt

References

Banh-Thien, T., H. Dang-Trung, L. Le-Anh, V. Ho-Huu, and T. Nguyen-Thoi. 2017. Buckling analysis of non-uniform thickness nanoplates in an elastic medium using the isogeometric analysis. *Composite Structures* 162:182-193.

Benlahcen, F., K. Belakhdar, M. Sellami, and A. Tounsi. 2018. Thermal buckling resistance of simply supported FGM plates with parabolic-concave thickness variation. *Steel and Composite Structures* 29 (5):591-602.

Bouguenina, O., K. Belakhdar, A. Tounsi, and E. A. Adda Bedia. 2015. Numerical analysis of FGM plates with variable thickness subjected to thermal buckling. *Steel Compos. Struct* 19 (3):679-695.

Chau-Dinh, T., Q. Nguyen-Duy, and H. Nguyen-Xuan. 2017. Improvement on MITC3 plate finite element using edge-based strain smoothing enhancement for plate analysis. *Acta Mechanica* 228 (6):2141-2163.

Chen, D., J. Yang, and S. Kitipornchai. 2015. Elastic buckling and static bending of shear deformable functionally graded porous beam. *Composite Structures* 133:54-61.

Buckling analysis of functionally graded porous variable thickness plates resting on Pasternak foundation
using ES-MITC3

Truong Thanh Nguyen et al.

Do, N.-T., and T. T. Tran. 2023. Random vibration analysis of FGM plates subjected to moving load using a refined stochastic finite element method. *Defence Technology*.

Do, N.-T., T. T. Tran, and Q.-H. Pham. 2023. A new finite-element procedure for vibration analysis of FGP sandwich plates resting on Kerr foundation. *Curved and Layered Structures* 10 (1):20220195.

Eisenberger, M., and A. Alexandrov. 2003. Buckling loads of variable thickness thin isotropic plates. *Thin-Walled Structures* 41 (9):871-889.

Fazzolari, F. A. 2018. Generalized exponential, polynomial and trigonometric theories for vibration and stability analysis of porous FG sandwich beams resting on elastic foundations. *Composites Part B: Engineering* 136:254-271.

Jalali, S., M. Naei, and A. Poorsolhjouy. 2010. Thermal stability analysis of circular functionally graded sandwich plates of variable thickness using pseudo-spectral method. *Materials & Design* 31 (10):4755-4763.

Javaheri, R., and M. Eslami. 2002. Buckling of functionally graded plates under in-plane compressive loading. *ZAMM-Journal of Applied Mathematics and Mechanics/Zeitschrift für Angewandte Mathematik und Mechanik: Applied Mathematics and Mechanics* 82 (4):277-283.

Kim, J., K. K. Żur, and J. Reddy. 2019. Bending, free vibration, and buckling of modified couples stress-based functionally graded porous micro-plates. *Composite Structures* 209:879-888.

Lee, P.-S., and K.-J. Bathe. 2004. Development of MITC isotropic triangular shell finite elements. *Computers & Structures* 82 (11-12):945-962.

Li, Q., D. Wu, X. Chen, L. Liu, Y. Yu, and W. Gao. 2018. Nonlinear vibration and dynamic buckling analyses of sandwich functionally graded porous plate with graphene platelet reinforcement resting on Winkler–Pasternak elastic foundation. *International Journal of Mechanical Sciences* 148:596-610.

Liu, G., T. Nguyen-Thoi, and K. Lam. 2009. An edge-based smoothed finite element method (ES-FEM) for static, free and forced vibration analyses of solids. *Journal of Sound and Vibration* 320 (4-5):1100-1130.

Matsunaga, H. 2000. Vibration and stability of thick plates on elastic foundations. *Journal of Engineering Mechanics* 126 (1):27-34.

Nguyen-Thoi, T. T. P. Q. 2020. T An edge-based smoothed finite element for free vibration analysis of functionally graded porous (FGP) plates on elastic foundation taking into mass (EFTIM). *Math Probl Eng* 7 (1):17.

Nguyen, T. T., T. H. Nguyen, T. T. Tran, and Q.-H. Pham. 2023. A New Finite Element Procedure for the Dynamic Analysis of BDFGS Plates Located on Pasternak Foundation Subjected to the Moving Oscillator Load. *Iranian Journal of Science and Technology, Transactions of Mechanical Engineering*:1-19.

Nguyen, V. C., T. T. Tran, T. Nguyen-Thoi, and Q.-H. Pham. 2022. A novel finite element formulation for static bending analysis of functionally graded porous sandwich plates. *Frontiers of Structural and Civil Engineering* 16 (12):1599-1620.

Omurtag, M. H., A. Özütok, A. Y. Aköz, and Y. OeZCELİKOeRS. 1997. Free vibration analysis of Kirchhoff plates resting on elastic foundation by mixed finite element formulation based on Gateaux differential. *International journal for numerical methods in engineering* 40 (2):295-317.

Pasternak, P. 1954. On a new method of analysis of an elastic foundation by means of two foundation constants. *Gos. Izd. Lit. po Strait i Arkh*.

Pham-Tien, D., H. Pham-Quoc, V. Tran-The, T. Vu-Khac, and N. Nguyen-Van. 2018. Transient analysis of laminated composite shells using an edge-based smoothed finite element method. Paper read at Proceedings of the International Conference on Advances in Computational Mechanics 2017: ACOME 2017, 2 to 4 August 2017, Phu Quoc Island, Vietnam.

Pham, Q.-H., P.-C. Nguyen, and T. T. Tran. 2022. Free vibration response of auxetic honeycomb sandwich plates using an improved higher-order ES-MITC3 element and artificial neural network. *Thin-Walled Structures* 175:109203.

Pham, Q.-H., T.-D. Pham, Q. V. Trinh, and D.-H. Phan. 2020. Geometrically nonlinear analysis of functionally graded shells using an edge-based smoothed MITC3 (ES-MITC3) finite elements. *Engineering with Computers* 36 (3):1069-1082.

Pham, Q.-H., T.-V. Tran, T.-D. Pham, and D.-H. Phan. 2018. An edge-based smoothed MITC3 (ES-MITC3) shell finite element in laminated composite shell structures analysis. *International Journal of Computational Methods* 15 (07):1850060.

Buckling analysis of functionally graded porous variable thickness plates resting on Pasternak foundation
using ES-MITC3

Truong Thanh Nguyen et al.

Pham, Q. H., T. T. Tran, A. M. Zenkour, and T. Nguyen-Thoi. 2023. Multi-objective optimization for free vibration of L-shaped bi-functionally graded sandwich plates using an effective finite element method and non-dominated sorting genetic algorithm II. *Composite Structures* 326:117622.

Ramu, I., and S. Mohanty. 2014. Buckling analysis of rectangular functionally graded material plates under uniaxial and biaxial compression load. *Procedia Engineering* 86:748-757.

Reddy, B. S., J. S. Kumar, C. E. Reddy, and K. Reddy. 2013. Buckling analysis of functionally graded material plates using higher order shear deformation theory. *Journal of composites* 2013.

Rezaei, A., and A. Saidi. 2016. Application of Carrera Unified Formulation to study the effect of porosity on natural frequencies of thick porous–cellular plates. *Composites Part B: Engineering* 91:361-370.

Saha, R., and P. Maiti. 2012. Buckling of simply supported FGM plates under uniaxial load. *International Journal of Civil and Structural Engineering* 2 (4):1035.

Shariat, B. S., and M. Eslami. 2007. Buckling of thick functionally graded plates under mechanical and thermal loads. *Composite Structures* 78 (3):433-439.

Thai, H.-T., and D.-H. Choi. 2012. An efficient and simple refined theory for buckling analysis of functionally graded plates. *Applied Mathematical Modelling* 36 (3):1008-1022.

Thai, H.-T., and S.-E. Kim. 2013. Closed-form solution for buckling analysis of thick functionally graded plates on elastic foundation. *International Journal of Mechanical Sciences* 75:34-44.

Thang, P. T., T. Nguyen-Thoi, D. Lee, J. Kang, and J. Lee. 2018. Elastic buckling and free vibration analyses of porous-cellular plates with uniform and non-uniform porosity distributions. *Aerospace science and technology* 79:278-287.

Thinh, T. I., T. M. Tu, T. H. Quoc, and N. V. Long. 2016. Vibration and buckling analysis of functionally graded plates using new eight-unknown higher order shear deformation theory. *Latin American Journal of Solids and Structures* 13:456-477.

Tran, T. T., and P. B. Le. 2023. Nonlocal dynamic response analysis of functionally graded porous L-shape nanoplates resting on elastic foundation using finite element formulation. *Engineering with Computers* 39 (1):809-825.

Tran, T. T., Q.-H. Pham, and T. Nguyen-Thoi. 2021. Static and free vibration analyses of functionally graded porous variable-thickness plates using an edge-based smoothed finite element method. *Defence Technology* 17 (3):971-986.

Vu, N. A., T. D. Pham, T. T. Tran, and Q.-H. Pham. 2023. Third-order isogeometric analysis for vibration characteristics of FGP plates in the thermal environment supported by Kerr foundation. *Case Studies in Thermal Engineering* 45:102890.

Winkler, E. 1867. *Die Lehre von der Elasticitaet und Festigkeit: mit besonderer Rücksicht auf ihre Anwendung in der Technik, für polytechnische Schulen, Bauakademien, Ingenieure, Maschinenbauer, Architecten, etc*: H. Dominicus.

Wu, D., A. Liu, Y. Huang, Y. Huang, Y. Pi, and W. Gao. 2018. Dynamic analysis of functionally graded porous structures through finite element analysis. *Engineering Structures* 165:287-301.

Wu, T.-L., K. Shukla, and J. H. Huang. 2007. Post-buckling analysis of functionally graded rectangular plates. *Composite Structures* 81 (1):1-10.

Xiang, Y., C. Wang, and S. Kitipornchai. 1994. Exact vibration solution for initially stressed Mindlin plates on Pasternak foundations. *International Journal of Mechanical Sciences* 36 (4):311-316.

Zenkour, A. 2005. A comprehensive analysis of functionally graded sandwich plates: Part 2—Buckling and free vibration. *International journal of Solids and Structures* 42 (18-19):5243-5258.

Zenkour, A. M. 2018. Bending of thin rectangular plates with variable-thickness in a hygrothermal environment. *Thin-Walled Structures* 123:333-340.